



Autonomous design framework for deploying building integrated photovoltaics

Qingxiang Li^a, Guidong Yang^{a,*}, Chenhong Bian^b, Lingege Long^c, Xinyi Wang^a,
Chuanxiang Gao^a, Choi Lam Wong^a, Yijun Huang^a, Benyun Zhao^a, Xi Chen^{a,*}, Ben M. Chen^a

^a Department of Mechanical and Automation Engineering, The Chinese University of Hong Kong, Hong Kong, China

^b School of Science and Technology, Hong Kong Metropolitan University, Hong Kong, China

^c School of Art and Design, Beijing Institute of Fashion Technology, Beijing 100029, China

HIGHLIGHTS

- A pipeline to reconstruct the buildings is developed.
- A explore-then-exploit algorithm for viewpoints path planning is provided.
- An autonomous framework for deploying BIPVs is provided.
- A component in Grasshopper is developed for BIPV economic assessment.

ARTICLE INFO

Keywords:

Path planning
3D modeling
Life cycle cost assessment
UAV
Solar potential

ABSTRACT

The advancements in perovskite solar cells present promising prospects for the widespread deployment of Building-Integrated Photovoltaics (BIPVs). Finding an efficient and accurate approach is essential to provide deployment strategies for decision support. This study develops an autonomous decision-making design framework for BIPV, including data collection, 3D modeling, and deployment strategy. For data collection, an open-source unmanned aerial vehicle platform is produced to execute an innovation explore-then-exploit algorithm for viewpoints generation and path planning. Subsequently, point cloud models of buildings are generated using a unique deep learning-based multi-view stereo network and then converted into polygonal surface models. Moreover, a novel Grasshopper plugin component is developed to assess the economic performance of various BIPV layouts by life cycle cost analysis. Based on the analysis results, potential BIPV deployment strategies are provided to support the decision-making process. The effectiveness of the framework is validated through its application in an industrial building in Hong Kong, demonstrating a 7.6 % discrepancy in the average annual solar radiation access value. Finally, two BIPV deployment strategies are proposed for the building. This study has significant implications for the design and deployment of PV systems in urban environments, representing an important step towards supporting the transition to sustainable and low-carbon cities.

Abbreviations: AASR, Average annual solar radiation; AC, Alternating current; ACVA, Adaptive cost volume aggregation; B, Batched volume; BIM, Building information modeling; BIPV, Building-integrated photovoltaic; C, Cost volume; c , Traversal cost; CAD, Computer-aided design; C_i , Cash inflows; CNN, Convolutional neural network; C_o , Cash outflows; D, Depth map; DC, Direct current; D_R , Discount rate; f , Deep feature; FPN, Feature pyramid network; GIS, Geographic information system; I, Image; K, Scaled intrinsic camera parameter; LCCA, Life cycle cost analysis; LiDAR, Light Detection and Ranging; MVS, Multi-view stereo; n , Lifetime of the BIPV system; NE, Northeast; NPV, Net present value; NW, Northwest; NURBS, Non-Uniform Rational Basis Splines; O&M, Operation and maintenance; P, Probability volume pyramid; p , Pixel; PCE, Power conversion efficiency; P_b , Predicted probability volume; $P_{l,gt}$, Ground-truth probability volume; PSC, Perovskite solar cell; PV, Photovoltaic; P_{view} , Generated path; R, Relative rotation; S, Matching score; SE, Southeast; SW, Southwest; t , Translation; UAV, Unmanned aerial vehicle; V, Feature volume; V_{free} , Unoccupied volume; V_{front} , Frontier volume; V_{occ} , Occupied volume; V_{un} , Uncovered volume; V_{view} , Viewpoint; α , Learnable parameter; β , Tunable balancing; λ , Loss weight; γ , Focusing parameter; \mathbb{R} , Real number set; Γ , Total loss; \odot , Hadamard product.

* Corresponding author.

E-mail addresses: gdyang@mae.cuhk.edu.hk (G. Yang), xichen002@cuhk.edu.hk (X. Chen).

<https://doi.org/10.1016/j.apenergy.2024.124760>

Received 27 May 2024; Received in revised form 11 September 2024; Accepted 16 October 2024

Available online 22 October 2024

0306-2619/© 2024 Elsevier Ltd. All rights reserved, including those for text and data mining, AI training, and similar technologies.

1. Introduction

It is reported that building sectors contribute almost 35 % of global energy consumption and 38 % of greenhouse gas emissions to the world [1]. In response, numerous nations have established targets to reduce building energy demand and have implemented corresponding measures [2]. Solar photovoltaic (PV) sources emerge as a promising solution to address the escalating energy needs of buildings and mitigate associated emissions in urban environments. PV panels can be seamlessly integrated onto the roofs and facades of existing building structures to form building-integrated photovoltaic (BIPV) systems [3]. The adoption of BIPVs holds significant promise for promoting sustainable and livable urban environments. Notably, lightweight perovskite solar cells (PSCs) with robust electrical performance have been enabled by recent technology advancement, even in shaded conditions, facilitating effective utilization of vertical facades as power sources [4]. Consequently, high-density urban areas have considerable potential to lead the widespread adoption of BIPV applications, addressing localized energy demands and fostering a more balanced energy landscape [5].

The urban environment poses distinct challenges to the widespread implementation of BIPV. Cityscapes exhibit a vertical and dense growth pattern to accommodate the increasing demand for space, resulting in significant shadowing effects and direct sun blockage [6]. Consequently, when deploying BIPV systems on specific buildings, evaluating solar potential and economic feasibility becomes imperative to formulate detailed and appropriate PV deployment strategies, facilitating informed decision-making support [7]. Designing a BIPV system for an existing building typically involves three key steps: building data acquisition, building 3D modeling, and assessment of BIPV deployment strategies. Each of these steps encounters unique challenges in achieving an efficient and automated process while ensuring accurate results.

1.1. BIPV design

BIPV system design is relevant to detailed building data [8]. In previous research about BIPV systems, the building data is always available for analysis [9–11]. But in practice, building data collection is always a tedious and time-intensive process. Establishing a BIPV project is challenging without accessible data and cost-effective solutions. Existing BIM-based platforms are often too complex for engineers and architects to effectively apply for early-stage feasibility assessments. The design for BIPV systems needs a comprehensive evaluation of technical [12] and economic [13] feasibility in their lifecycle. Factors such as product specifications, building data, and PV layout, which significantly influence energy generation and investment, must be taken into account. Designing a BIPV system involves exploring a variety of design combinations to identify the optimal solution [14].

Among various factors, economic investigation on BIPVs through Life cycle cost analysis (LCCA) is crucial for exploring optimal BIPV designs during the conceptual design phase [15]. LCCA stands as an economic assessment method aimed at determining the comprehensive cost of owning and operating a system in a specified period [16]. Corti et al. [17] employed a comprehensive economic evaluation, utilizing the net present value method. A sensitivity analysis was developed to assess costs by varying key economic input parameters that significantly impact the financial aspects of BIPV installations. Li et al. [18] presented a circular economy approach for implementing PSCs in vertical building envelopes and evaluates its economic feasibility through a LCCA in Europe. The study compared the economic performance of PSC envelopes with that of conventional rigid BIPV systems. Quintana et al. [19] presented an integrated simulation using BIM-friendly software to evaluate the techno-economic performance of a BIPV system in a Swedish building cluster. The study highlights the competitiveness of BIPV integration in terms of both economic investment and energy potential. However, the economic model employed omits critical financial and technical factors, such as discount rates and PV degradation, which

limit the precision of the results. Grasshopper, Rhino as a parametric modeling software can assess the solar potential of building by the 3D model, then LCCA is used for the economic feasibility of BIPV systems [20]. But the calculation process of LCCA is always complicated due to numerous parameters, resulting in practitioners in different field have to be involved even in the early stages of the project. A grasshopper component is better to create, which can operate the LCCA process automatic in Rhino.

1.2. Data collection

The data applied for building reconstruction can be categorized based on the obtained data type [21]. Ranging-based and image-based sensors are the two of the most commonly used type to obtain data [22]. Ranging-based data are expensive to obtain and require professional techniques [23]. Image-based sensors are more accessible and suitable for BIPV deployment strategies. One critical factor for the following 3D modeling is the pixel-wise visibility, determining whether a 3D point is observable within specific images [24]. Nevertheless, visibility information remains unavailable until dense recovery of the 3D model is completed. This issue is particularly pronounced in building reconstruction within high-density urban environments, where obstructions from surrounding buildings and narrow gaps pose challenges for aerial photography. In this context, effective unmanned aerial vehicle (UAV) path planning becomes critical. Developing an exploration method that can rapidly gather data about the target building and its surroundings is essential in such complex environments. UAVs have proven to be a powerful tool for building data acquisition [25]. Although commercial UAV products have been commonly applied by researchers for scanning, yet they cannot integrate algorithms for special requirements in advanced tasks. An open-source UAV platform therefore becomes necessary.

Previous studies have either developed viewpoints and paths offline or relied on initial models sourced from aerial image data, Google Earth, or GIS data for path planning purposes [26]. Phung et al. [27] formulated the building scanning path planning problem as a traveling salesman problem and validated their approach using open datasets. Similarly, Tan et al. [28] proposed an integrated method combining BIM and UAV technologies to enable automatic scanning. In their approach, the inspection path planning problem is addressed using a genetic algorithm based on the available BIM model. Nevertheless, in practical 3D modeling applications, digital models of both the target building and its surrounding infrastructures are often unavailable in the early stage. Designing an exploration method capable of swiftly gathering data for the reconstruction of the target building and its surroundings becomes paramount.

1.3. 3D modeling

3D building models have traditionally been employed for visualization purposes, yet there is a growing acknowledgment among BIPV practitioners of their benefits to support decision-making. [29]. A pivotal rationale behind this trend is that the representation of our surroundings in 3D format, as opposed to 2D maps and drawings, is generally more intuitive and easier to grasp, thus serving as an effective tool for communication and information sharing [30]. 3D building models assume a crucial role in the analysis and management of building and urban data, as evidenced by the plethora of applications using this information. One of the very first attempts is presented by Lewis and Séquin [31] who introduced a semi-automatic method to construct 3D polyhedral building models from floor plans in CAD software, demanding minimal user intervention. Within the timeframe of a few days, they successfully generated a cohesive model of a building comprising over 300 rooms from initial 2D data.

Considerable research efforts have been directed towards automating the collection of 3D data and reconstructing objects to attain

greater fidelity [32–36]. Typically, the financial and temporal investments required for the development of intricate 3D building models are substantial, escalating as the desired level of detail increases [37]. As a result, it is necessary to find alternative cost-effective methods to offer viable solutions within this background. An increasing number of researchers have developed a range of modeling technologies to generate 3D information for evaluating the solar potential of urban areas [38–43]. Currently, modeling techniques can generally be classified into two categories: image-based modeling and point cloud-based modeling [21].

The majority of image-based modeling approaches rely on 2D maps, typically inserted into GIS platform [32]. Thebault [41] proposed a GIS-based method for classifying rooftop PV suitability in large cities, aimed at evaluating the feasibility of PV systems on an urban scale. Certainly, with the aid of GIS, additional information can be incorporated, enabling the generation of 2.5D building models. 2.5D models is a convenient and efficient approach to exploiting a district model in GIS based software. In GIS-based models, various algorithms and methods have been proposed; however, they all involve significant simplifications in building geometry. This is because façades are typically generated using elevation data, neglecting their detailed dimensions [44].

Point cloud-based methods for generating 3D modeling employ topographic information and aerial images to collect essential data such as building shape and dimensions [21]. Salimzadeh et al. [38] integrated point clouds with BIM to optimize the factors of PV panels, aiming to maximize solar radiation access. Suomalainen [39] generated a digital surface model of an urban area using LiDAR data to estimate annual solar radiation on rooftops. The model accounts for shading effects caused by nearby buildings and trees, providing a more accurate assessment of solar potential. However, relying exclusively on LiDAR technology to obtain key parameters of buildings and their surroundings presents certain limitations such as the high cost and low efficiency in data acquisition as well as loss of surface textures.

In recent years, learning-based approaches for point cloud reconstruction have proved considerable advantages over traditional techniques [45–48]. However, a significant challenge remains in the implementation of these learning-based methods. Many of these approaches utilize a feature pyramid network (FPN) to capture image features [49]. Nonetheless, a prevalent problem encountered in these approaches is the tendency to generate excessively smoothed depth estimations, particularly around object boundaries [48]. This smoothing phenomenon is primarily attributed to the lack of shallow feature information, which encompasses low-level details.

Accurate 3D modeling methods are a fundamental step in achieving this goal. Generally, traditional 3D modeling is manual work, which is always time consuming and labor-intensive task [24]. Also, the dimensions of surrounding buildings are not easy to access which increase communication cost. An automatous 3D modeling approach is required to develop the building models rapidly for the following BIPV design.

1.4. Research objective

Herein, this study aims to develop an autonomous framework for BIPV system design in conceptual stage. To achieve this objective, three innovative tasks need to be conducted:

- a. An open-source UAV platform is designed and constructed to conduct an innovative explore-then-exploit path planning for data collection, which ensures comprehensive coverage of the target buildings and enables online data collection without the necessity of a pre-existing 3D model of the target structure.
- b. For 3D modeling, a novel point cloud reconstruction method is developed using aerial images. Surface modeling is performed using PolyFit and City3D, and the resulting surface model is further processed in Rhino to create editable 3D models for subsequent assessments.

- c. In terms of PV design assessment, a grasshopper-plugged component is firstly developed to assess the BIPV deployment strategies using life cycle cost analysis.

The proposed framework increases the efficiency of building 3D modeling, especially for the objects in high-density urban environment, and enhances the accuracy of solar potential assessment. Finally, different BIPV deployment strategies can be offered to support decision-making process. The paper is structured as follows: Section 2 provides the methodology of the proposed framework. In section 3, a case study is provided. Then, the modeling results and layout strategies are shown in Section 4. Discussions about the limitation and future work are shown in Section 5 and conclusions are presented Section 6.

2. Methodology

This study aims at developing an automatous decision-support framework for BIPV design, including data collection, 3D modeling, and deployment strategy. The output of the framework comprises 3D models, which are generated by processing images and geographic coordinate system data collected by UAVs. These models are instrumental in assessing solar potential, economic feasibility, and deployment strategies within Grasshopper, Rhino.

As illustrated in Fig. 1, the framework follows three main steps. First, an open-source UAV platform and a viewpoint path planning algorithm are developed to enable explore-then-exploit scanning for reconstruction without relying on a pre-obtained 3D model of the target building. Next, a novel Learnable Cost Metric-based Multi-view Stereo Network is employed to convert aerial images into point cloud models of buildings within the district. The modeling targets two objectives: accurately modeling the target building for solar potential assessment and BIPV deployment, and capturing the surrounding buildings, which affect the solar radiation access of the target structure.

For the target building, precise and detailed modeling of dimensions and shape is critical to improve the accuracy of subsequent assessments. However, modeling all surrounding buildings with equal precision significantly reduces efficiency. In this study, it is assumed that a finely reconstructed model of the bottom-half of surrounding buildings has minimal impact on the solar potential assessment of the target building in a high-density urban environment. Aerial video footage is captured only from the roof level, which results in missing details of the lower portions of surrounding buildings in the point cloud reconstruction. City3D is then used to convert the surrounding buildings' point clouds into surface models, with an algorithm introduced to reconstruct vertical planes and address the missing details. Next, the solar radiation on the target building is evaluated using the Ladybug Grasshopper plugin. Two distinct strategies for BIPV system deployment are considered: one focuses on meeting the building's energy demand, while the other evaluates the economic performance of the BIPV system, using an innovative Grasshopper plugin component for life cycle cost analysis. Finally, these deployment strategies are compared to support informed decision-making.

2.1. Data collection

Commercial UAV products typically lack the capability to integrate custom path planning algorithms. Consequently, we developed an open-source UAV platform specifically tailored for scanning target buildings and their surrounding environments.

The UAV equipped with cameras and sensors collects visual and depth data from the environment. These measurements are then utilized to construct a volumetric map in which surfaces are distinguished as unoccupied $v \in V_{free}$, occupied $v \in V_{occ}$, or uncovered $v \in V_{un}$. Collectively, the map is constituted by the integration of three voxel subsets: $M = V_{free} \cup V_{occ} \cup V_{un}$. To generate a coverage path encompassing the unexplored surfaces of a building, we refer to the method

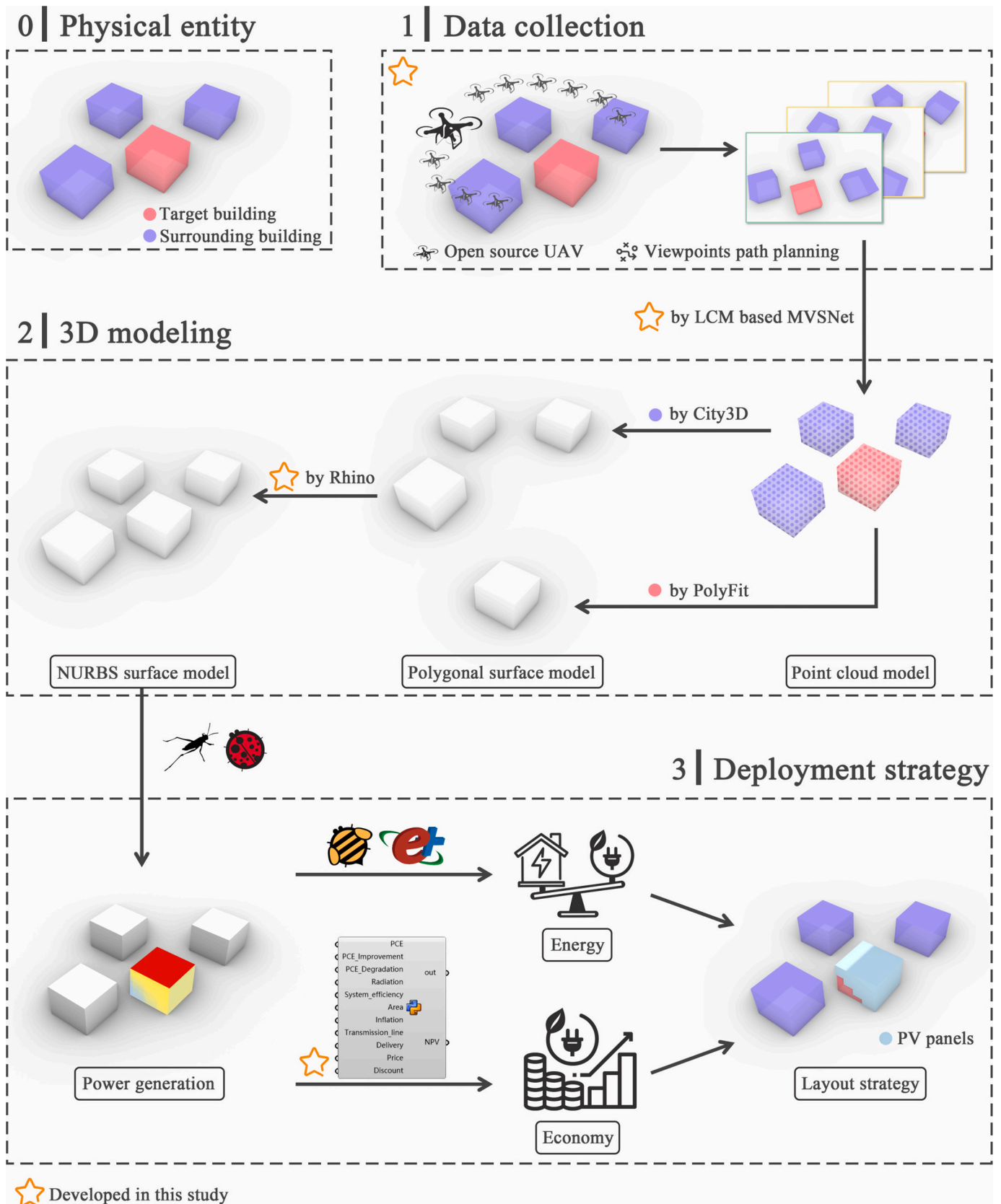


Fig. 1. Framework of the study.

mentioned in [24]. A clustering algorithm leveraging Euclidean distance and surface normal vectors is utilized to classify the uncovered surfaces, identifying the $V_{front} = \{V_1, \dots, V_N\}$ frontier clusters requiring observation. Subsequently, dual sampling is applied to derive feasible four-degree-of-freedom viewpoints, designating a cover region that guarantees the visibility of the target cluster $V_i, i \in 1, \dots, N$.

Following the dual sampling process, the viewpoint within each cluster that displays the maximum surface visibility ratio is chosen to form the set $V_{view} = \{v_1, v_2, \dots, v_N\}$, where each viewpoint is defined by its spatial coordinates and the yaw angle. Determining the shortest path traversing each viewpoint from the present position can be modeled as the Asymmetric Traveling Salesman Problem. We establish v_{ij} represents the connectivity between viewpoints v_i and v_j , and the traversal cost c_{ij} is the expense of traveling between given viewpoints i and j . The optimization objective is to minimize the aggregate traversal distance across all viewpoints:

$$\min \sum_{i=1}^N \sum_{j=1}^N c_{ij} v_{ij} \quad (1)$$

After solving this optimization problem, the UAV will follow the generated paths P_{view} through all these viewpoints to collect the images of the target building. The algorithm for viewpoints path planning is shown in Table 1.

2.2. 3D modeling

In this study, the reverse 3D modeling includes three steps. The first step is to generate 3D point cloud model by Learnable Cost Metric based MVSNet. Then, the 3D point cloud reconstruction model is converted to polygonal surface model. For the target building, the polygonal surface model is created by Polyfit. For the surrounding structures, the polygonal surface model is generated by City3D. Finally, the model is fed into Rhino software to produce NURBS surface model. After trimming, the model is prepared for simulation in Grasshopper.

2.2.1. Point cloud reconstruction

LCM based MVSNet is an innovative deep learning-based point cloud reconstruction approach, which can develop the 3D point cloud model of the buildings in the target district. LCM scheme is applied to balance heuristic and learning-based cost volume aggregation. Traditional heuristic methods overlook scene variations across different views. LCM addresses this by computing the per-view significance to account for these variations. To mitigate memory and computational demands inherent in learning-based aggregation methods, LCM incorporates sparse point hints from structure-from-motion into the aggregation process. This approach allows for the direct computation of source-view significance and the learning of reference-view significance from training data. Consequently, the LCM scheme adapts to multi-view scene variations while reducing computational burden.

The approach is tailored for large-scale district reconstruction based on the following coarse-to-fine depth estimation paradigm. A series of unordered images $\{I_i\}_{i=0}^N$ are provided from $N + 1$ viewpoints, then the depth map D_0 is estimated for the reference image I_0 with N neighboring source images $\{I_i\}_{i=1}^N$. Sequentially, the input images are treated iteratively as the reference image to anticipate per-view depth maps $\{D_i\}_{i=0}^N$. These depth maps are then fused to form the ultimate point cloud

Table 1

The algorithm for viewpoints path planning.

Algorithm 1: Viewpoints Path Planning
Input: Volumetric map M
Output: Coverage Path P_{view}
$\{V_1, \dots, V_N\} \leftarrow \text{FrontierClustering}(M);$
$\{v_1, \dots, v_N\} \leftarrow \text{GlobalSampling}(\{V_1, \dots, V_N\});$
$P_{view} \leftarrow \text{SolveATSP}(\{v_1, \dots, v_N\});$

reconstruction. The network (Fig. 2) has five steps as follows:

Enhanced multi-scale feature pyramid extraction Given multi-view images $\{I_i\}_{i=0}^N$, the feature pyramid network (FPN) is leveraged to extract multi-scale $(L + 1)$ -level features $\{f_{l,i} \in \mathbb{R}^{F_l \times H/2^l \times W/2^l}\}_{l=0}^L$ for each input image I_i , where F_l is the channel number.

Sparse Point-Guided Adaptive Cost Volume Aggregation One feature level l is provided, we can obtain the deep features $f_{l,i}$. The depth range $[d_{min,l}, d_{max,l}]$ can be separated into the 3D space. Because multi-view stereo is able to solve pixel correspondences across multi-view images, homography is used to match corresponding pixel between feature map in the reference view $f_{l,0}$ and feature map in the source view $f_{l,i}$. Each $d_{m,l}$ determines a homography between the pixel in the reference view $p_{l,0}$ and the i -th pixel in the source view $p_{l,i}$.

$$p_{l,i} = K_i [R(K_0^{-1} p_{l,0} + t)] \quad (2)$$

where K_0 and K_i represent the scaled intrinsic camera parameters for the reference and the i -th source view. The variables R and t denote the relative rotation and translation between the two views. To establish feature correspondence, differentiable bilinear interpolation is used for pixel sampling from $f_{l,i}$, where $p_{l,i}$ specifies the pixel location.

Following the feature warping process, the warped feature maps are concatenated along the depth dimension, resulting in the creation of the source-view feature volume $V_{l,i} \in \mathbb{R}^{F_l \times M_l \times H/2^l \times W/2^l}$ for the i -th source view. Additionally, we replicate the reference feature map $f_{l,0}$ ($M + 1$) times along the depth dimension, producing the reference-view feature volume $V_{l,0}$.

Next, the proposed Sparse ACVA is used to adaptively aggregate multi-view feature volumes into a single cost volume C_l . The Sparse ACVA is set as follows:

$$\begin{aligned} C_l &= M(V_{l,0}, \dots, V_{l,N}) \\ &= M(B_{l,0}, \dots, B_{l,N}) \\ &= \text{AvgPool} \left(\alpha_l B_l, 0 \odot \sum_{i=1}^N \frac{S_i}{\sum_{i=1}^N S_i} B_{l,i} \right) \end{aligned} \quad (3)$$

where $B_{l,i} \in \mathbb{R}^{K \times (F_l/K) \times M_l \times H/2^l \times W/2^l}$ stands for the batched volumes. At various network levels, denoted as $l \in \{0, 1, \dots, L\}$, distinct learnable values are assigned to α_l to capture the significance of the reference view. Moreover, the normalized matching score $S_i / \sum_{i=1}^N S_i$ is applied as the source-view significance, in order to make the MVSNet to adjust to the scene change. \odot stands for the Hadamard product.

Cost Volume Regularization and Continuous Depth Estimation A 3D convolutional neural network (CNN) is used to regularize the aggregated cost volume pyramid $\{C_l\}_{l=0}^L$ and create the probability volume pyramid $\{P_{l,est}\}_{l=0}^L$ by the sigmoid activation function. To achieve continuous depth estimation, the discrete depth estimation is improved by the following method:

$$D_{l,est} = \underset{dm,l \in [d_{min,l}, d_{max,l}]}{\operatorname{argmax}} \left(P_{l,est}(dm, l) + \frac{(d_{max,l} - d_{min,l})}{Ml} \max_{dm,l} P_{l,est}(dm, l) \right) \quad (4)$$

where $P_{l,est}(dl)$ is the probability map at depth hypothesis dl . $D_{l,est}$ is the depth estimation at level l . $\operatorname{argmax}_{dm,l \in [d_{min,l}, d_{max,l}]} P_{l,est}(dm, l)$ is the discrete depth. $(d_{max,l} - d_{min,l})/Ml$ is the depth interval. $\max_{dm,l} P_{l,est}(dm, l)$ is the normalized bias.

Loss Function To achieve normalized depth residual, we modify the generalized focal loss to oversee the dissimilarity between the predicted probability volume P_l and the ground-truth probability volume $P_{l,gt}$. The computation of $P_{l,gt}$ involves determining the normalized depth residual between the ground-truth depth and the discrete depth hypothesis. The total loss is weighted as:

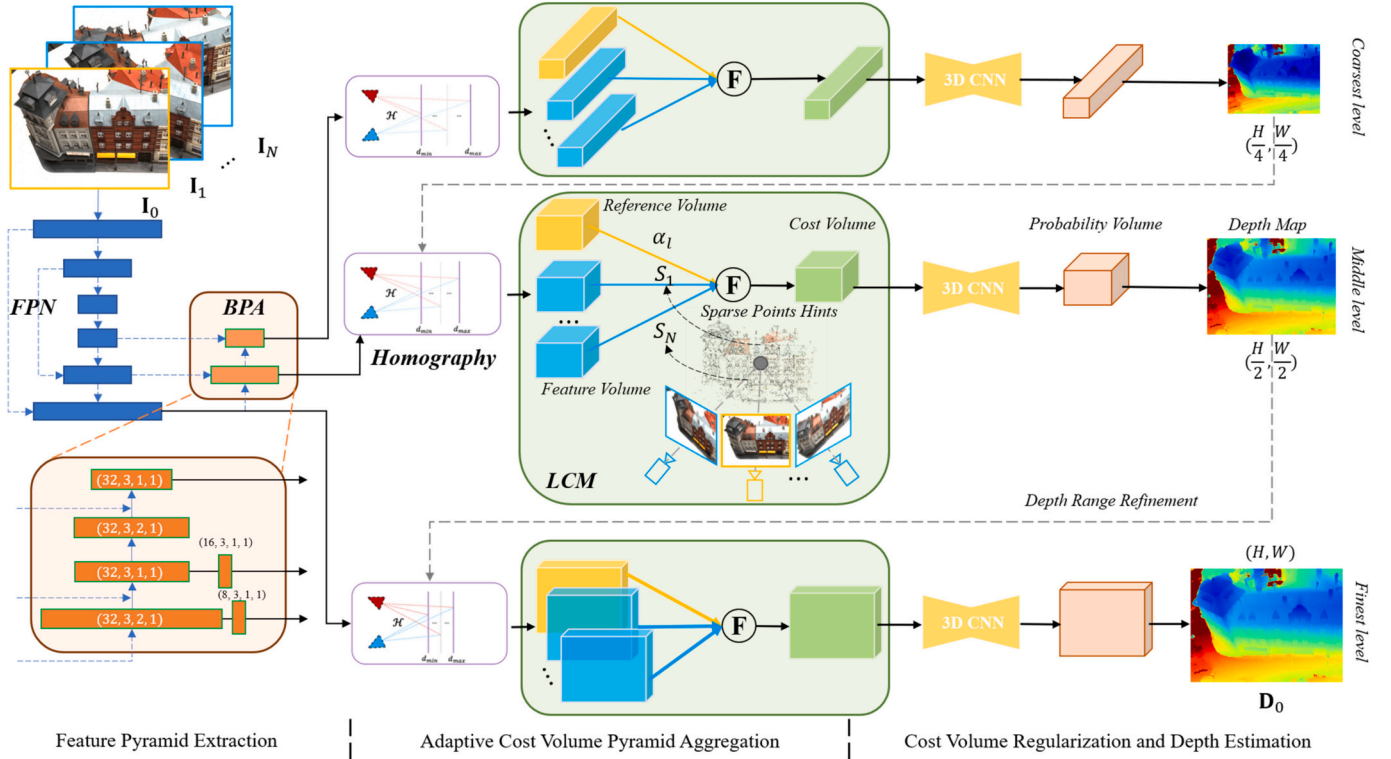


Fig. 2. Overview of the LCM based MVSNet.

$$\Gamma l = \sum_{x \in \{x_{\text{valid}}\}} -\beta |Pl, gt(x) - Pl, est(x)|^l. \quad (5)$$

$$((1 - Pl, gt(x)) \log(Pl, est(x)) + Pl, gt(x) \log(Pl, est(x)))$$

and

$$\Gamma = \sum_{l=0}^L \lambda \Gamma l \quad (6)$$

Depth Map Fusion Using a set of multi-view depth maps $\{D_i\}_{i=0}^N$, depth map is filtered in order to avoid depth outliers and enforce the criterion of consistent views N_c to ensure depth consistency. Finally, the filtered multi-view depth maps are emerged to develop the final point cloud model.

2.2.2. Lightweight polygonal surface reconstruction

PolyFit method is applied to develop polygonal surface reconstruction from point clouds. The PolyFit is to generate lightweight polygonal surface models from point cloud datasets, particularly in scenarios where the data might be noisy, incomplete, or contain outliers. The methodology is divided into two main phases: Candidate face generation and Face selection.

The proposed method for generating polygonal surface models from point cloud data encompasses a multi-phase process. Firstly, in the Candidate face generation phase, planar segments are identified utilizing the Random Sample Consensus (RANSAC) algorithm, followed by an iterative refinement procedure to mitigate noise and outliers. These refined planes serve as the basis for hypothesizing the object's faces. Subsequently, in the Face selection phase, an optimal subset of candidate faces is selected to form a manifold and watertight polygonal surface model. This phase employs binary linear programming, incorporating an objective function that considers data fitting, point coverage, and model complexity, alongside hard constraints for manifold and watertight properties. To tackle noise and outliers, the initial RANSAC-based method undergoes iterative refinement, and pairwise intersections of clipped planes are computed. The optimization-based

face selection guarantees the selection of confident faces while adhering to specified constraints. Energy terms within the objective function quantify data fitting, model complexity, and point coverage. The resulting polygonal surface model accurately depicts the object while preserving manifold and watertight characteristics, demonstrating the method's effectiveness even in challenging scenarios.

2.2.3. District-scale polygonal surface reconstruction

Existing approaches to urban building reconstruction aim to achieve detailed representations and automate processes suitable for extensive urban areas. Consequently, methods with aerial photography typically depend on comprehensive building coverage to acquire high-fidelity data inputs. However, the processing of such high-quality data places significant demands on computer memory resources for executing the reconstruction algorithms. Consequently, these methods face limitations in their applicability to district-scale scenarios where rapid reconstruction is essential. Conversely, for BIPV deployment on individual buildings, detailed reconstruction of the target structure suffices. Surrounding structures only require rudimentary profiles, devoid of intricate details, to facilitate solar radiation access simulations.

In the dense urban environment, when scanning the surrounding structures of the target building for reconstruction, the moving route of the aerial scanner is always planned above the building for oblique photography to achieve efficient scanning. Because of the limited positioning and flying space of UAVs, the bottom-half part of vertical walls of buildings cannot be captured by the scanners. Incomplete data make challenge for the polygonal surface reconstruction by Polyfit.

In this study, the City3D polygonal surface reconstruction method is used to solve the problem. The City3D is improved for the district-scale reconstruction based on the PolyFit, introducing a method to fix vertical facades from incomplete point clouds to fix the missing bottom part of the building point cloud. Through the integration of these two types of planar primitives, the building surfaces are hypothesized. The ultimate model is then derived by selecting the optimal building surfaces via an optimization process. To ensure the method work well, three hard rules

are added during the optimization process, including single-layer roof and face prior.

The method takes in a raw point cloud of an extensive urban setting along with the associated building footprints as input. Initially, the method collects the footprint polygon of each structure. Next, it infers the vertical planes based on the already known structure, leading to the formation of a height map. Following this step, contours can be collected from the height map by the Canny detector [46], enable to estimate of the vertical surfaces of the building. Polyline can be inferred from the contours by an optimization method. Subsequently, a condensed polygonal surface model is reconstructed from the point cloud model. Finally, the 3D polygonal surface models can be obtained to show the buildings.

2.2.4. NURBS surface model in rhino

Rhino can address both mesh and NURBS surface (Non-Uniform Rational Basis Splines). NURBS serves as a mathematical framework for representing 3D geometry. In essence, it provides a method for crafting smooth, intricate shapes within 3D modeling. A NURBS surface consists of ‘control points’ that dictate its overall form and structure. The polygonal surface reconstruction model of the target building as an object are input to the rhino and the object can be converted to mesh surfaces in the rhino. The utilization of mesh for simulation within Grasshopper often leads to the occurrence of bugs. Conversely, the NURBS surface model exhibits flawless simulation capabilities within Grasshopper. Consequently, it is necessary to explore a method to convert the surfaces from mesh to NURBS surface.

The Surface Patch method is used to convert irregular mesh geometries into trimmed surfaces, offering a viable solution where conventional methods may fall short. The implemented process follows a step-by-step approach, beginning with mesh deconstruction, followed by surface fitting, subsequent trimming, and ultimately achieving accurate surface representations. By leveraging the Patch component, which interpolates surfaces through a given set of points, the method accommodates non-rectangular and irregular mesh boundaries, ensuring a

comprehensive surface coverage. Furthermore, the integration of Mesh Edges and Surface Split components enables the generation of trim curves and subsequent surface division, facilitating the selection of the most appropriate surface representation. This method highlights its efficacy in producing precise, trimmed surfaces from complex mesh geometries, contributing to the advancement of computational design methodologies.

2.3. Deployment strategy

This study applied two methods to obtain the BIPV deployment strategies. One considers economic performance of the BIPV system. The other one considers the balance of the building energy consumption and BIPV power generation. The analyses are conducted in grasshopper, rhino (in Fig. 3).

2.3.1. Solar potential assessment and building energy simulation

Generally, solar potential is categorized into three distinct classifications: geographic, physical, and technical. Geographic potential stands for the available area suitable for integrating PV panels. Physical potential stands for the total solar radiation received by the panels. Technical potential quantifies the electricity output achievable from the solar PV system, factoring in its efficiency and performance characteristics.

For the target building, the roof and vertical façades are all considered to be available for the PV deployment. The solar radiation on PV panels is analyzed by Ladybug plugin’s Radiance engine based on the generated 3D models, thus the computation of PV energy production can be calculated. PSC module is employed with 15 % PCE. The conversion efficiency from direct current (DC) to alternating current (AC) is set at 85 % [91]. The effective area of the solar cell is 0.7.

Building energy is simulated in Honeybee, a plugin of Rhinoceros using the EnergyPlus engine. In this study, the calculation of building energy consumption is performed for the target building. The building function for the block is uniformly set as industrial buildings.

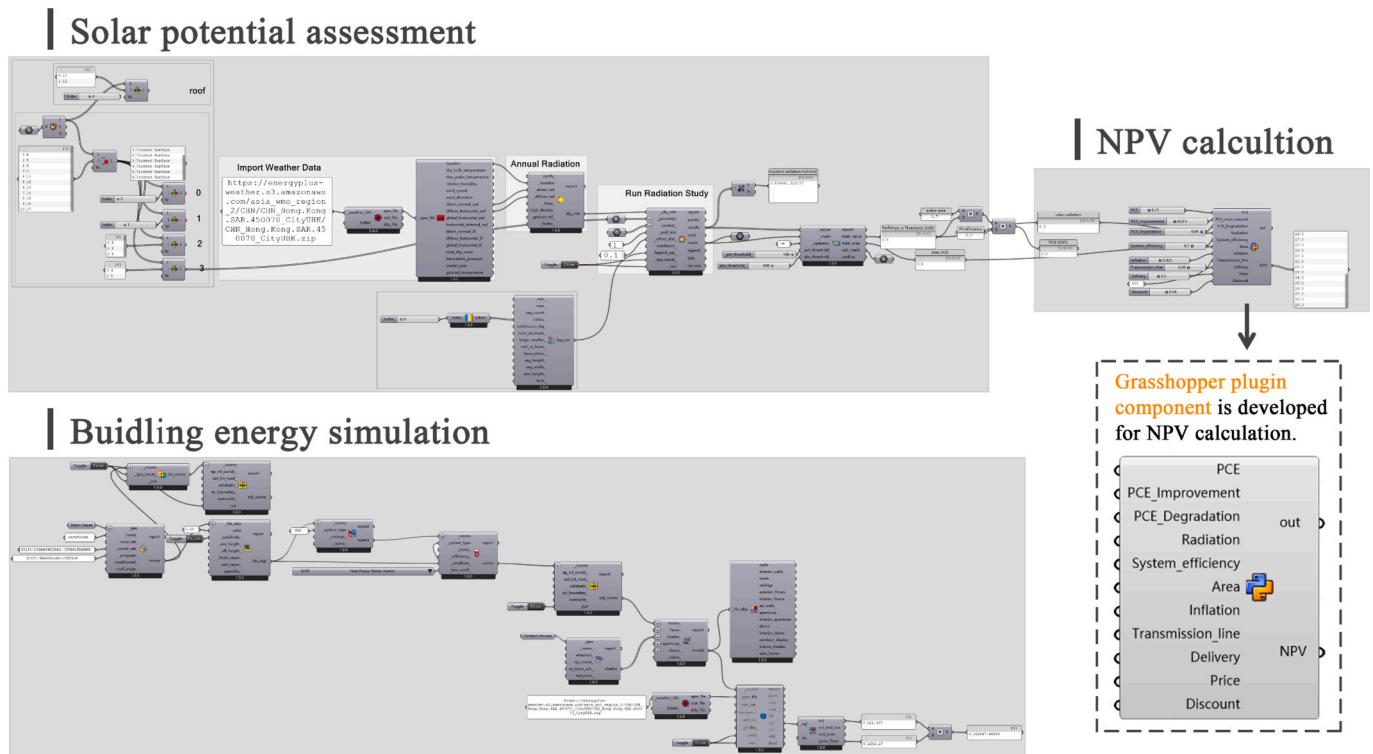


Fig. 3. Analysis workflow in grasshopper and the component developed for NPV calculation.

2.3.2. NPV calculation

Previous studies have suggested annual solar radiation thresholds of 1000 kWh/m²/year and 800 kWh/m²/year as benchmarks for PV power generation on building roofs and vertical envelopes, respectively. Areas receiving annual solar radiation exceeding these thresholds are deemed suitable for PV deployment. However, due to variations in locations, types of PV systems, and associated costs, a fixed threshold may not adequately guide all scenarios.

A custom Grasshopper component is created for economic feasibility assessment based on life cycle cost analysis. The component is written using Python, a language that supports a wide range of tasks through its extensive library ecosystem. The component analyzes the economic feasibility using LCCA method. LCCA serves as a methodological approach to gauge the economic efficacy of the target system. Presently, Grasshopper lacks a built-in capability or plugin to automate the calculation of LCCA outcomes for BIPV systems. This investigation introduces the component designed to automate the LCCA computation process. The component comprises two sections: (1) a Grasshopper front-end with one Grasshopper Python Script component, and (2) an IronPython back-end. For the front-end, the power generation calculation under shadow conditions is considered based on author's previous research [12]. The front-end functions as a user interface, gathering user inputs, transmitting them to the back-end, and displaying the output parameters. The inputs include solar radiation access, BIPV area, PV specifications, and economic parameters. Consequently, the Grasshopper component contains a minimal amount of Python code, accessible by double-clicking a component in Grasshopper. The Python back-end code handles all calculations and data generation. The outputs include electricity generation and NPV.

Net Present Value (NPV) is a common metric used to illustrate the net financial advantages of a system throughout its lifecycle. It represents the disparity between the profits and the whole spences incurred by the product over its lifespan. The calculation method is presented as the following equation:

$$NPV = \sum_{t=1}^n (CI - CO)(1 + DR)^t \quad (7)$$

where C_i stands for cash inflows. D_R , n stand for discount rate and life-time of the BIPV system.

In this study, initial investment, operation and maintenance (O&M) cost, replacement cost, and electricity sale income are considered. For initial investment, material cost (PSCs, inverters, and other components) and personnel cost are considered. Generally, the personnel cost is set as 20 % of the total material cost. The O&M costs are approximated at around 0.5 % of the initial investment per annum. Replacement costs account for both inverter and photovoltaic solar cell replacements, with the assumption that replacement prices match the initial purchase prices in the first year. Electricity sale income constitutes a vital component,

influenced by both power generation and the prevailing local electricity prices.

3. Case study

An industrial building (Fig. 4) is in a high-density urban area of Hong Kong (22.40°N, 114.19°E). Due to its function, the vertical façades are minimally adorned with windows, rendering the entirety of the façade available for the installation of PV panels. In 2021, the Government unveiled Hong Kong's Climate Action Plan 2050, with a primary focus on “energy saving and green buildings” as one of key decarbonization strategies. In this context, the government selects this building as a pilot BIPV project. However, the surrounding environment poses a complex challenge. The building is surrounded by high-rise residential buildings and storehouses. Prior to implementation of BIPV, cost-optimal deployment strategies should be analyzed to inform decision-making for investors and officials based on the proposed automatous framework.

This study adopts a default angle of 20°. Regarding the roof availability coefficient, values typically fluctuate between 0.3 and 0.5, with variations dependent on the land use characteristics in urban areas [50]. Given the study's emphasis on a storehouse within the district, the roof availability coefficient for this specific urban land use is set to 0.4. Regarding the price of PV panels, the cost of mono-Si PV panels is derived from prevailing market rates. Additionally, the price for the PSC is intricately linked to the purchasing quantity of PSC and adheres to the model outlined in existing literature [51]. The lifespan of the system is set at 5 years. The current electricity price for distributed PV systems is set to: 4 HK dollar for system power generation capacity equal to or less than 10 kW; 3 HK dollar for system power generation capacity greater than 10 kW but not exceeding 200 kW; 2.5 HK dollar for system energy production capacity greater than 200 kW but not exceeding 1 MW. In the context of Hong Kong, the D_R is deemed to be 4 %. Consequently, the beginning year for LCCA calculation in this study is 2021, with the analysis extending until 2050.

4. Results

In this section, the results are shown and analyzed based on the proposed framework.

4.1. Viewpoints path planning

We implemented modules for area sensing, viewpoints generating, and path planning on our UAV platform. Beginning from one point near the target building, the UAV automatically navigates to designed load-balanced areas based on reconstruction metrics derived from a density map. As the UAV progresses, it gradually expands its coverage to encompass additional building areas until reaching optimal regions. Our

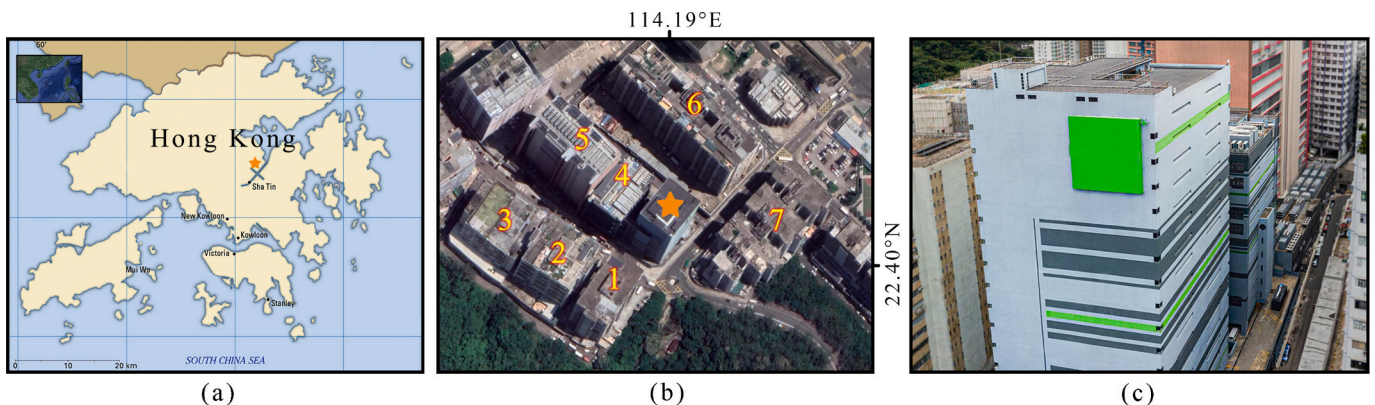


Fig. 4. (a) Location of the building. (b) The target building (star marked) and surrounding buildings. (c) The target industrial building.

path planning strategy promotes decentralized exploration of uncharted areas, ensuring safety during dynamic coverage operations within dense urban environments. Once optimal regions are identified, the UAV captures images of the building, and viewpoints are established above the building roof. The planned aerial viewpoints for both the target building are depicted in Fig. 5. Despite occasional instability of GPS and localization uncertainty, the UAV successfully completed reconstruction tasks using our proposed framework. We compared the scanning method proposed by this study to the method proposed by [28]. Our method employs an explore-then-exploit scanning approach and does not require a BIM model of the target structure, addressing the issue of inaccessible building data. In terms of data collection speed, both methods demonstrated similar completion times. However, our approach does not require presetting viewpoints and paths before scanning. The 12 min include the time allocated for the UAV to autonomously explore and determine optimal viewpoints and paths after takeoff.

4.2. Point cloud reconstruction

We successfully reconstructed the 3D point cloud model of the target building and its surrounding structures using the proposed LCM-based MVSNet, as illustrated in Fig. 6. Additionally, Fig. 7 shows the depth maps exhibit enhanced smoothness of edges and distinct boundaries.

The results present a complete reconstruction of the target building. Furthermore, for the surrounding buildings, most structures that influence the solar radiation access of the industrial building have been fully reconstructed. Moreover, the data collected by the low-flying UAV yield complete point clouds of buildings in the horizontal direction, particularly on the roofs. Unlike other 3D point cloud reconstruction methods, our approach ensures dense point clouds on vertical façades, even capturing shallow feature information such as textures and edges. This is attributed to the bottom-up pathway introduced in the proposed LCM-based MVSNet, which minimizes parameter increases and accelerates the propagation of shallow information, enhancing both depth estimation and reconstruction. However, it should be noted that the southeast wall of building 7 is absent in the model due to missing GPS signals, resulting in the UAV's inability to scan this area. Additionally, Fig. 8 presents aerial pictures and corresponding depth maps in eight different perspectives. The depth maps exhibit smooth edges and sharp boundaries compared to the aerial images. This study also explored the performance of Metashape and Colmap in reconstructing the cloud point model of the district. Colmap failed the reconstruction task as it required more memory to process the same number of photos. The reconstructed point cloud result by Metashape was shown in the Fig. S1. It can be found that the model quality is noticeably lower than that generated by our LCM-based MVSNet. The model generated by Metashape exhibits noticeable disproportions, influencing the assessment in the following steps. For the reconstruction speed, LCM-based MVSNet spends 11.783

mins on NVIDIA RTX 3090Ti GPU. On the same device, Metashape spends 15.238 mins to reconstruct the model.

4.3. Polygonal surface reconstruction

In this step, the point cloud model of the target building was transformed into a polygonal surface model using Polyfit (Fig. 8), while the point cloud model of the surrounding structures was converted into a polygonal surface model using City3D. Subsequently, these polygonal surface models were imported into Rhino software and converted into NURBS surface models.

For the generated model of the target building, a balance between data-fitting, model complexity, and point coverage was made using the Polyfit software. Given the completeness and uniformity of the imported point clouds of the industrial building, the weight of point coverage (used to address missing data due to occlusions) was set lowest among the three factors. Data-fitting (assessing the quality of fitting faces to the point cloud) and complexity (to prevent gaps and encourage simple structures) were deemed more critical for the accuracy of the reconstructed model, hence they were given higher weights. A comparison between the actual size of the building and the size of the generated model revealed an error of 1.54 % and 1.02 % in the building façade area and roof area. This discrepancy can be attributed to the reference distance measured on-site and the conversion process from point clouds to polygonal surfaces.

For the surrounding buildings, a tradeoff between fitting, complexity, and height was made while being converted to surface model in software City3D. The level of details of the surrounding buildings is not important for the solar potential assessment of the target building. The dimensions of the surrounding buildings are more important. The height of the building 1–7 were compared with the actual height of the buildings, shown in Fig. 8. An error occurred during the conversion process of building 2 and building 3. The results indicate that these two buildings were merged into a single polygonal surface model. This issue arose due to the methodology employed by City3D, which identifies building footprints. Given the close proximity of building 2 and building 3, compounded by the complexity of the surrounding environment, the software recognized their footprints as belonging to a single building. Moreover, it can be found that deviation of building 6 is far larger than other buildings. This disparity can be attributed to a slope present in different building façades, with the model generated according the height on the higher road side. The absolute error between the elevation of the actual roof and the model roof was found to be only 1.2 m.

4.4. BIPV deployment strategy

Based on the reconstructed NURBS surface model, the solar radiation access of the target building was assessed in the ground-truth model and

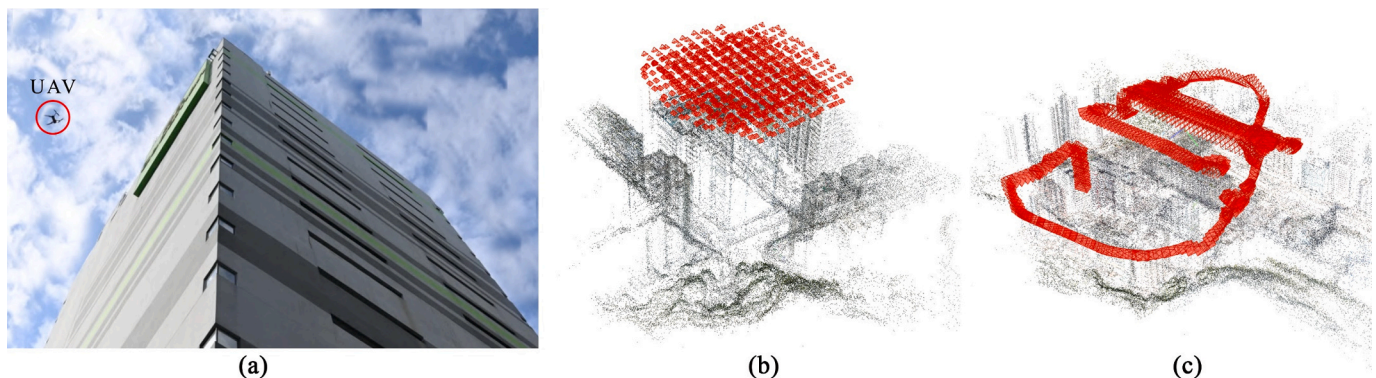


Fig. 5. Data collection. (a) Scanning by UAV. (b) Viewpoints for the industrial building scanning. (c) Route for the district scanning.



Fig. 6. The point cloud model of the target building and surrounding buildings reconstructed by LCM based MVSNet.

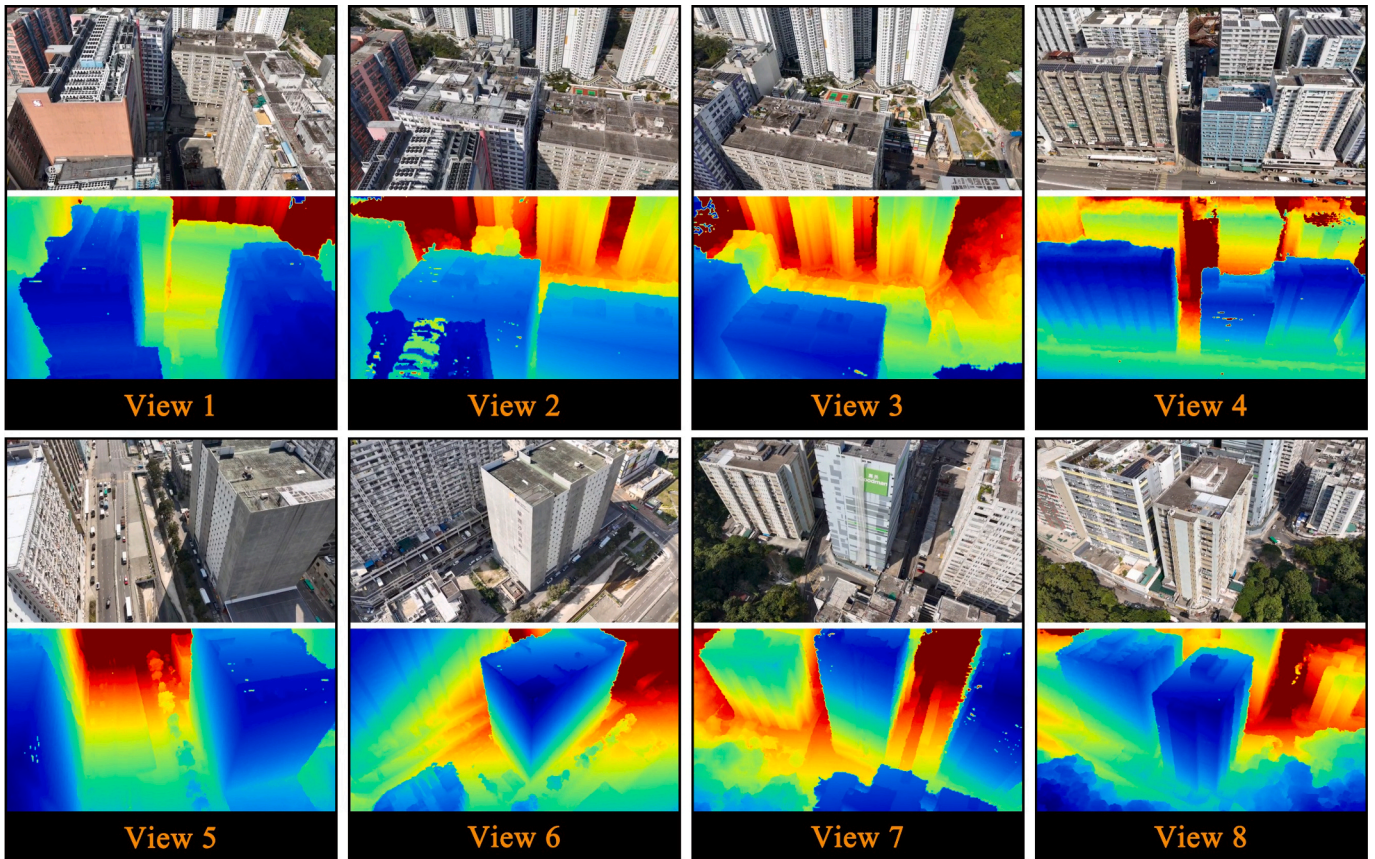


Fig. 7. The aerial images and corresponding depth maps.

reconstructed model (Fig. 9). The average annual solar radiation access of the target building in the true model is 345.7 kWh/m^2 . The average solar radiation access per year of the target building in the reconstructed model is 371.2 kWh/m^2 . Also, a more accurate method is used to identify the accuracy of the distribution of the solar radiation on each façade. The surface models of the ground-truth model and the reconstructed model are converted to 20,906 points with three-dimensional coordinate and solar radiation values. The accuracy is calculated to

compare the solar radiation value S of the point G in the ground-truth model and point R in the reconstructed model, whose Euclidean distance is shortest. Then iterate this computation over all points, from where the mean value is identified as accuracy.

$$e_{r-g} = |S_r - S_g| \left(\min_{g \in G} \|r - g\|_2 \right) \quad (8)$$

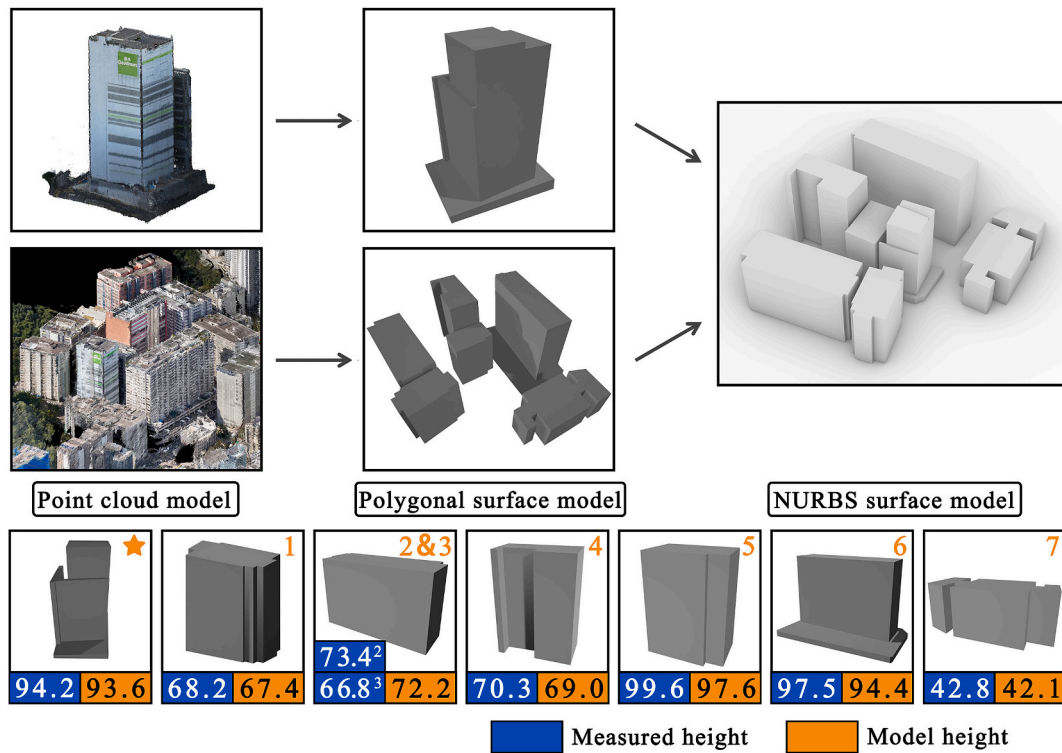


Fig. 8. The polygonal surface model and NURBS surface model. The measured heights and model heights of building.

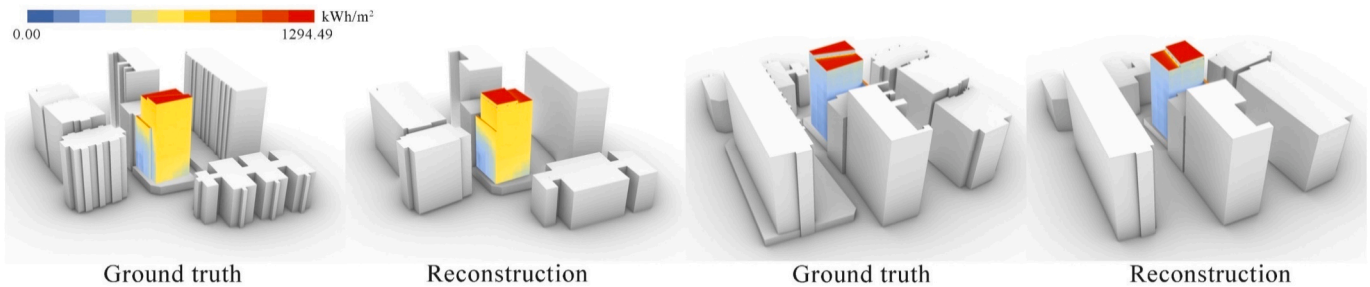


Fig. 9. Comparison of the solar radiation access in the true model and reconstructed model.

$$Accuracy = \frac{1}{|R|} \sum_{r \in R} [e_{r \rightarrow G} < d] e_{r \rightarrow G} \quad (9)$$

where $\|\cdot\|_2$ represents the Euclidean distance. $|\cdot|$ stands for point number. $[\cdot]$ denotes the Iverson bracket. d is the outlier rejection threshold. The results show that the accuracy of the reconstructed model is 0.0014 kWh/m².

Fig. 10 illustrates the solar radiation distribution of the building envelope under varying thresholds. The design of BIPV systems is predicated on the distribution of solar radiation. Based on the simulation results, it was found that the average annual solar radiation on most of the building facade is below 700 kWh/m². Consequently, we selected an annual solar radiation range of >200->600 kWh/m² to illustrate the varying areas suitable for BIPV applications under different settings.

Power generation distributions of BIPV systems were computed, alongside the calculation of NPVs under various thresholds of solar radiation access for different orientations. The results substantiate the efficacy of the framework in providing diverse BIPV layouts based on simulated solar radiation distributions on the reconstructed model. Moreover, the NPV of BIPV systems on each facade serves as a guiding metric for BIPV deployment, aiding the decision-making process. Analysis of NPV results reveals that the northeast facade is not

conducive to BIPV application, as substantial profits cannot be realized. Conversely, for the southeast facade, where most areas receive over 600 kWh/m² of solar radiation, BIPV systems designed based on varying thresholds exhibit similar NPV results, indicating that economic considerations are less critical for this facade during PV panel deployment. In contrast, on the southwest facade, NPV increases with higher solar radiation thresholds. Lastly, for the northwest facade, areas receiving 300–500 kWh/m² of solar radiation emerge as the most suitable for PV deployment. From the NPV results, it can be found that the southeast facade application has a payback period of 8 years, with total benefits reaching up to 10 M HK dollars within 30 years. For the southwest facade, installing PSCs in areas receiving more than 600 kWh/m² can also result in a short payback period of 8 years, with an NPV of 6.7 M HK dollars. The northwest facade can generate 1.4 M HK dollars when PSCs are installed in areas receiving more than 400 kWh/m². These NPV results are comparable to those reported in [52], which utilized a hybrid energy system, and both studies yield results within the same order of magnitude, proving the completeness of the PSC facade.

The proposed framework presents two solutions (as seen in Fig. 11) for the BIPV deployment of the target building, focusing on profit maximization and energy supply optimization. In the profit-maximizing strategy, the objective is to maximize the NPV of the BIPV system.

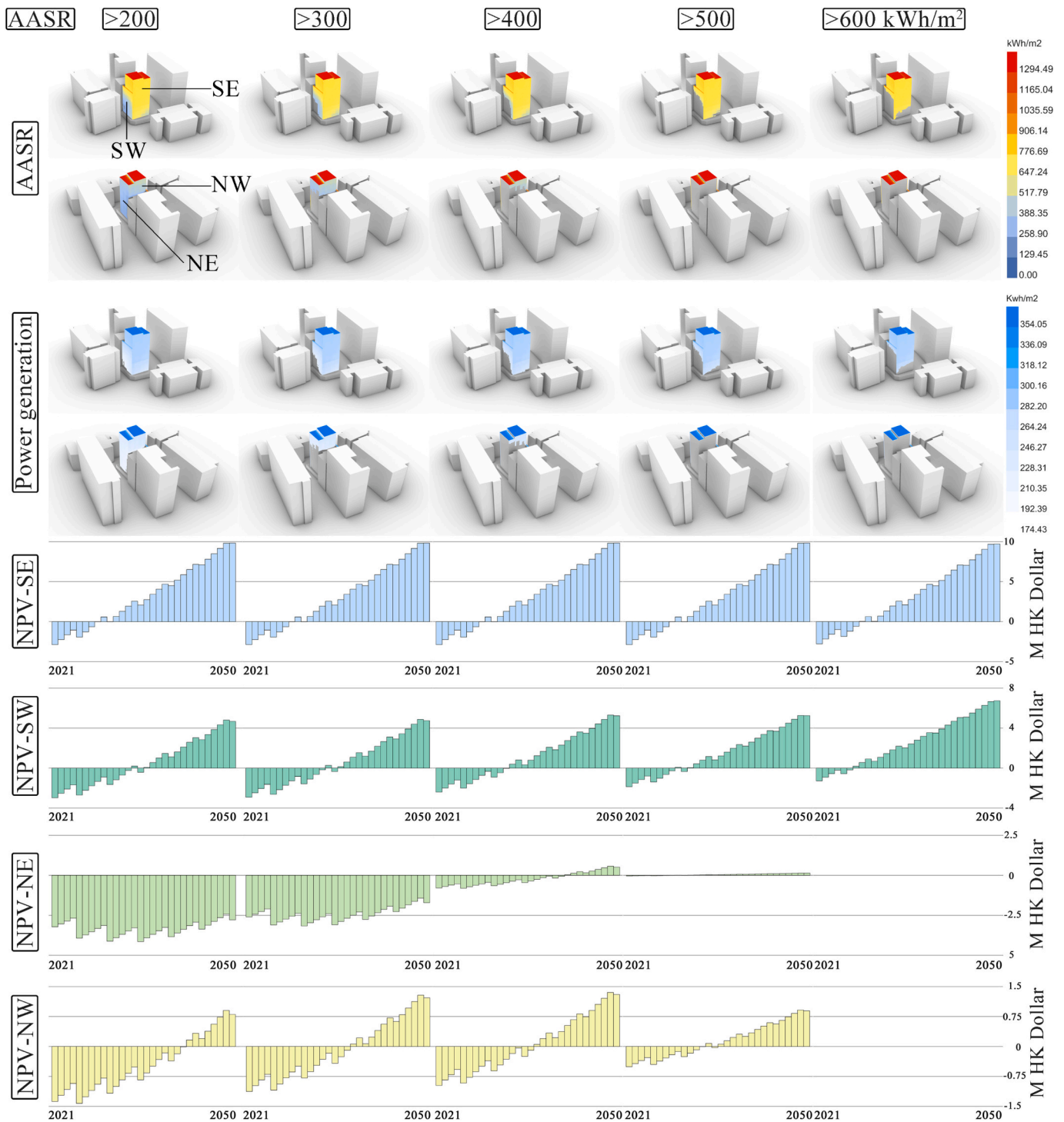


Fig. 10. Average annual solar radiation (AASR) distribution of the building envelope, power generation of BIPV systems, and NPV of BIPV in different orientation under varying AASR setting.

According to the analysis, the entire SE facade is designated for PSC deployment, while the NE facade is excluded. For the SW facade, BIPV deployment is selected for areas receiving solar radiation over 608 kWh/m² of solar radiation, while the threshold for PSC deployment on the NW facade is set as 384 kWh/m². Regarding energy supply, this study targets to fulfill 50 % of the building’s energy demand through the BIPV system as a corresponding solution. The entirety of the SE facade is allocated for PSC deployment, and the threshold for PSC deployment on the NE facade is set as 292 kWh/m². For the SW and NW facades, BIPV should be deployed on areas receiving solar radiation over 336 kWh/m² and

324 kWh/m² respectively.

5. Discussion

In the 3D modeling, errors come from the generation and conversion process. It’s crucial to recognize that any conversion process will inevitably entail a trade-off between accuracy, speed, or usability of the resulting output. It should be noted that this framework is not suitable for the building with curved surfaces. For curved surface, the differences in the construction methods of meshes and surfaces present certain

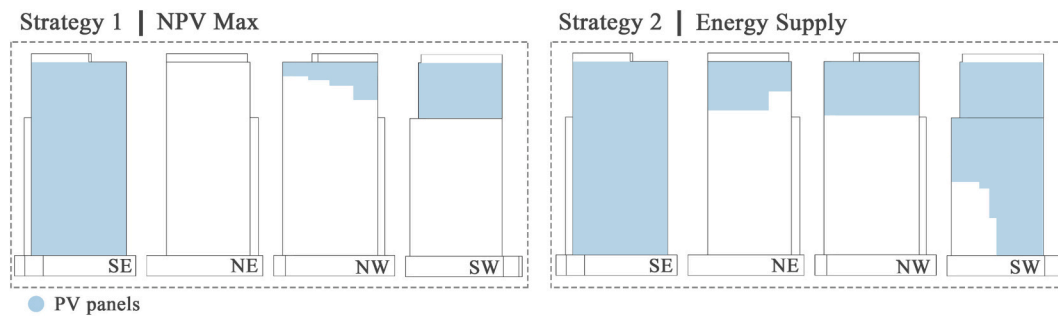


Fig. 11. BIPV layout strategies based on the proposed framework.

challenges when attempting to convert between the two. While converting polygonal surface to NURBS surface, the resulting NURBS surface is clearly an approximation of the original polygonal surface. The primary challenge arises from the fact that meshes and surfaces utilize distinct 3D reference points for generating their geometry: vertices for meshes and control points for surfaces. This discrepancy in reference points can lead to noticeable deviations, particularly depending on the source mesh and the method of surface subdivision. In this study, the polygonal surface models generated by Polyfit and City3D can only be flat, fitting in with the requirement of subsequent simulations and avoiding the errors incurred from the conversion process. But for buildings with curved envelope, the conversion error becomes a major concern. Although the processes of point cloud reconstruction and polygonal surface reconstruction both show errors, they have little influence on the final assessment of BIPV system based on generated 3D models.

In this study, we used Polyfit to generate the surface model of the industrial building and also compared its performance with other approaches, including DualCont [53] and ManBox [54]. PolyFit was adopted as it presents an effective balance between accuracy and compactness. The accuracy and compactness are most important for the target building reconstruction to conduct deployment strategy assessment. It shows the bottlenecks only when encountering computation for large complex objects, which rarely become targets for BIPV applications. PolyFit is therefore selected to complete the framework. For Dualcont, the model generated by Dualcont shows a relatively larger numbers of faces, which likely increase the error in the conversion from polygonal surfaces to NURBS surfaces. For ManBox, it is unstable in reconstructing the building structures, resulting in larger deviations. For the surface model reconstruction of surrounding structures, City3D is used for the reconstruction of building surfaces. One shortcoming is that the program can only address building footprint data. Before importing the point cloud model to City3D, the point cloud model is required to extract the building roof information, which adds to the complexity of the process.

In the future work, we will develop a fully autonomous end-to-end approach to convert the scanning aerial images directly to surface model, which could help to improve the accuracy of the modeling process. Then, the reconstruction approach will be packaged as a software tool to provide an easy operation workflow. Also, for the economic feasibility of BIPV deployment strategy, we will integrate more economic indicators (levelized cost of energy [9], discounted payback period [18], and internal rate of return [13]) into the grasshopper component to provide more information to support decision-making. Moreover, more constraints will be considered from the perspective of society and environment in the modeling process. The environmental impacts of the proposed BIPV strategies will be assessed by life cycle assessment [55]. And an immersive VR like research [56] will be developed to collect the opinions of local citizens on the BIPV strategies.

6. Conclusions

This study developed an autonomous framework to provide BIPV deployment strategies for decision making in early design stage. The framework has three steps, including data collection, 3D modeling, and deployment strategy. The framework was applied in an industrial building in Hong Kong to validate the effectiveness.

For data collection, an open-source unmanned aerial vehicle platform was produced to execute an innovation explore-then-exploit algorithm for viewpoints generation, and path planning. The results showed the method can ensure comprehensive coverage of the target buildings and enables online data collection without the necessity of a pre-existing 3D model of the target structure.

Based on the collected data, the point cloud models of the target building and surrounding structures were built by a unique deep learning-based multi-view stereo network to realize precise and rapid reconstruction. The results presented a complete point cloud reconstruction of the target building. The depth maps exhibited smoother edges and sharper boundaries compared to the aerial images.

These models were then converted into polygonal surface models, then into NURBS surface model, which was simulated in grasshopper to obtain solar radiation distribution of the building envelope. The results indicated a 7.6 % discrepancy between the value of average annual solar radiation access of the target building in the true model and that in the reconstructed model. Furthermore, the accuracy of the solar radiation distribution in the reconstructed model was analyzed by a Euclidean distance method. The framework showed that the accuracy of the annual solar radiation distribution is 0.0014 kWh/m².

Moreover, a novel component in Grasshopper was developed to assess the economic performance of various BIPV layouts by life cycle cost analysis. Based on the analysis results, two potential BIPV deployment strategies from the perspective of profits and energy supply were provided to support the decision-making process. The findings of this study carry significant implications for the design and deployment of BIPV systems within urban landscapes, marking a crucial stride towards fostering the development of sustainable and low-carbon cities.

CRedit authorship contribution statement

Qingxiang Li: Writing – original draft, Visualization, Validation, Methodology, Investigation, Formal analysis, Conceptualization. **Guidong Yang:** Investigation. **Chenhong Bian:** Investigation. **Lingege Long:** Investigation. **Xinyi Wang:** Investigation. **Chuanxiang Gao:** Investigation. **Choi Lam Wong:** Investigation. **Yijun Huang:** Investigation. **Benyun Zhao:** Investigation. **Xi Chen:** Writing – review & editing, Supervision, Funding acquisition. **Ben M. Chen:** Investigation.

Declaration of competing interest

The authors declare that they have no known competing financial interests or personal relationships that could have appeared to influence

the work reported in this paper.

Data availability

Data will be made available on request.

Acknowledgement

This work was sponsored by the InnoHK of the Government of the Hong Kong Special Administrative Region via the Hong Kong Centre for Logistics Robotics. Appreciation is also given to the CUHK Direct Grant for Research No. 4055168 and the Research Grants Council of the Hong Kong Special Administrative Region, China (UGC/FDS16/E04/21).

Appendix A. Supplementary data

Supplementary data to this article can be found online at <https://doi.org/10.1016/j.apenergy.2024.124760>.

References

- Andersen I. *United Nations Environment Programme* 2023. 2023.
- Prataviera E, Zarella A, Morejohn J, Narayanan V. Exploiting district cooling network and urban building energy modeling for large-scale integrated energy conservation analyses. *Appl Energy* 2024;356:122368. <https://doi.org/10.1016/j.apenergy.2023.122368>.
- Wijeratne WMPU, Samarasinghalage TI, Yang RJ, Wakefield R. Multi-objective optimisation for building integrated photovoltaics (BIPV) roof projects in early design phase. *Appl Energy* 2022;309:118476. <https://doi.org/10.1016/j.apenergy.2021.118476>.
- Walker L, Hofer J, Schlueter A. High-resolution, parametric BIPV and electrical systems modeling and design. *Appl Energy* 2019;238:164–79. <https://doi.org/10.1016/j.apenergy.2018.12.088>.
- Ding L, Zhu Y, Zheng L, Dai Q, Zhang Z. What is the path of photovoltaic building (BIPV or BAPV) promotion? –The perspective of evolutionary games. *Appl Energy* 2023;340:121033. <https://doi.org/10.1016/j.apenergy.2023.121033>.
- Li Q, Monticelli C, Kutlu A, Zanelli A. Environmental performance analysis of textile envelope integrated flexible photovoltaic using life cycle assessment approach. *Journal of Building Engineering* 2024;89:109348. <https://doi.org/10.1016/j.job.2024.109348>.
- Xu Z, Matsui T, Matsubara K, Sai H. Effect of multilayer structure and surface texturing on optical and electric properties of structural colored photovoltaic modules for BIPV applications. *Appl Energy* 2024;367:123347. <https://doi.org/10.1016/j.apenergy.2024.123347>.
- Wu Z, Kang J, Mosteiro-Romero M, Bartolini A, Ng TS, Su B. A distributionally robust optimization model for building-integrated photovoltaic system expansion planning under demand and irradiance uncertainties. *Appl Energy* 2024;372:123740. <https://doi.org/10.1016/j.apenergy.2024.123740>.
- Li Q, Li T, Kutlu A, Zanelli A. Life cycle cost analysis and life cycle assessment of ETFE cushion integrated transparent organic/perovskite solar cells: comparison with PV glazing skylight. *Journal of Building Engineering* 2024;87:109140. <https://doi.org/10.1016/j.job.2024.109140>.
- Ito R, Lee S. Development of adjustable solar photovoltaic system for integration with solar shading louvers on building façades. *Appl Energy* 2024;359:122711. <https://doi.org/10.1016/j.apenergy.2024.122711>.
- Jing Y, Zhu L, Yin B, Li F. Evaluating the PV system expansion potential of existing integrated energy parks: a case study in North China. *Appl Energy* 2023;330:120310. <https://doi.org/10.1016/j.apenergy.2022.120310>.
- Li Q, Zhu L, Sun Y, Lu L, Yang Y. Performance prediction of building integrated photovoltaics under no-shading, shading and masking conditions using a multi-physics model. *Energy* 2020;213:118795. <https://doi.org/10.1016/j.energy.2020.118795>.
- Li Q, Monticelli C, Kutlu A, Zanelli A. Feasibility of textile envelope integrated flexible photovoltaic in Europe: carbon footprint assessment and life cycle cost analysis. *J Clean Prod* 2023;430:139716. <https://doi.org/10.1016/j.jclepro.2023.139716>.
- Zhou Y-P, Wang L-X, Wang B-Y, Chen Y, Ran C-X, Wu Z-B. Polarization management of photonic crystals to achieve synergistic optimization of optical, thermal, and electrical performance of building-integrated photovoltaic glazing. *Appl Energy* 2024;372:123827. <https://doi.org/10.1016/j.apenergy.2024.123827>.
- Chen Q, Kuang Z, Liu X, Zhang T. Optimal sizing and techno-economic analysis of the hybrid PV-battery-cooling storage system for commercial buildings in China. *Appl Energy* 2024;355:122231. <https://doi.org/10.1016/j.apenergy.2023.122231>.
- Long L, Li Q, Gan Z, Mu J, Overend M, Zhang D. Life cycle assessment of stone buildings in the Taihang mountains of Hebei province: evolution towards cleaner production and operation. *J Clean Prod* 2023;399:136625. <https://doi.org/10.1016/j.jclepro.2023.136625>.
- Corti P, Follo A, Bonomo P. Workflow to support cost-benefits comparison and sensitivity analysis of BIPV case studies: three examples of BIPV facades in the south of Switzerland. *Energ Build* 2024;322:114732. <https://doi.org/10.1016/j.enbuild.2024.114732>.
- Li Q, Chen Z, Li X, Brancart S, Overend M. Vertical perovskite solar cell envelope for the circular economy: a case study using life cycle cost analysis in Europe. *J Clean Prod* 2024;467:143017. <https://doi.org/10.1016/j.jclepro.2024.143017>.
- Quintana S, Huang P, Saini P, Zhang X. A preliminary techno-economic study of a building integrated photovoltaic (BIPV) system for a residential building cluster in Sweden by the integrated toolkit of BIM and PVSITES. *Intell Build Int* 2021;13:51–69. <https://doi.org/10.1080/17508975.2020.1765134>.
- Costa A, Ng TS, Su B. Long-term solar PV planning: an economic-driven robust optimization approach. *Appl Energy* 2023;335:120702. <https://doi.org/10.1016/j.apenergy.2023.120702>.
- Li Q, Yang G, Gao C, Huang Y, Zhang J, Huang D, et al. Single drone-based 3D reconstruction approach to improve public engagement in conservation of heritage buildings: a case of Hakka Tulou. *Journal of Building Engineering* 2024;87:108954. <https://doi.org/10.1016/j.job.2024.108954>.
- Zhao B, Zhou X, Yang G, Wen J, Zhang J, Dou J, et al. High-resolution infrastructure defect detection dataset sourced by unmanned systems and validated with deep learning. *Autom Constr* 2024;163:105405. <https://doi.org/10.1016/j.autcon.2024.105405>.
- Yang G, Liu K, Zhang J, Zhao B, Zhao Z, Chen X, et al. Datasets and processing methods for boosting visual inspection of civil infrastructure: a comprehensive review and algorithm comparison for crack classification, segmentation, and detection. *Constr Build Mater* 2022;356:129226. <https://doi.org/10.1016/j.conbuildmat.2022.129226>.
- Feng C, Li H, Gao F, Zhou B, Shen S. PredRecon: A prediction-boosted planning framework for fast and high-quality autonomous aerial reconstruction. In: 2023 IEEE international conference on robotics and automation (ICRA). London, United Kingdom: IEEE; 2023. p. 1207–13. <https://doi.org/10.1109/ICRA48891.2023.10160933>.
- Song C, Chen Z, Wang K, Luo H, Cheng JCP. BIM-supported scan and flight planning for fully autonomous LiDAR-carrying UAVs. *Autom Constr* 2022;142:104533. <https://doi.org/10.1016/j.autcon.2022.104533>.
- Shujuan H, Wenqi C, Beixuan L, Feng X, Chao S, Wenjuan Z. An improved BAT algorithm for collaborative dynamic target tracking and path planning of multiple UAV. *Comput Electr Eng* 2024;118:109340. <https://doi.org/10.1016/j.compeleceng.2024.109340>.
- Phung MD, Quach CH, Dinh TH, Ha Q. Enhanced discrete particle swarm optimization path planning for UAV vision-based surface inspection. *Autom Constr* 2017;81:25–33.
- Tan Y, Li S, Liu H, Chen P, Zhou Z. Automatic inspection data collection of building surface based on BIM and UAV. *Autom Constr* 2021;131:103881.
- Nouvel R, Zirak M, Coors V, Eicker U. The influence of data quality on urban heating demand modeling using 3D city models. *Comput Environ Urban Syst* 2017;64:68–80. <https://doi.org/10.1016/j.compenvurbsys.2016.12.005>.
- Boulch A, Marlet R. POCO: point convolution for surface reconstruction. *Proceedings of the IEEE/CVF Conference on Computer Vision and Pattern Recognition (CVPR)* 2022:6302–14.
- Lewis R, Séquin C. Generation of 3D building models from 2D architectural plans. *Comput Aided Des* 1998;30:765–79. [https://doi.org/10.1016/S0010-4485\(98\)00031-1](https://doi.org/10.1016/S0010-4485(98)00031-1).
- Fath K, Stengel J, Sprenger W, Wilson HR, Schultmann F, Kuhn TE. A method for predicting the economic potential of (building-integrated) photovoltaics in urban areas based on hourly radiance simulations. *Sol Energy* 2015;116:357–70. <https://doi.org/10.1016/j.solener.2015.03.023>.
- Johari F, Lindberg O, Ramadhani UH, Shadram F, Munkhammar J, Widén J. Analysis of large-scale energy retrofit of residential buildings and their impact on the electricity grid using a validated UBEM. *Appl Energy* 2024;361:122937. <https://doi.org/10.1016/j.apenergy.2024.122937>.
- Chen Z, Yang B, Zhu R, Dong Z. City-scale solar PV potential estimation on 3D buildings using multi-source RS data: a case study in Wuhan. *China Applied Energy* 2024;359:122720. <https://doi.org/10.1016/j.apenergy.2024.122720>.
- Zhao Q, Zhou L, Lv G. A 3D modeling method for buildings based on LiDAR point cloud and DLG. *Comput Environ Urban Syst* 2023;102:101974. <https://doi.org/10.1016/j.compenvurbsys.2023.101974>.
- Liu W, Zang Y, Xiong Z, Bian X, Wen C, Lu X, et al. 3D building model generation from MLS point cloud and 3D mesh using multi-source data fusion. *Int J Appl Earth Obs Geoinf* 2023;116:103171. <https://doi.org/10.1016/j.jag.2022.103171>.
- Rashdi R, Martínez-Sánchez J, Arias P, Qiu Z. Scanning technologies to building information modelling: a review. *Infrastructures* 2022;7:49. <https://doi.org/10.3390/infrastructures7040049>.
- Salimzadeh N, Hammad A. High-level framework for GIS-based optimization of building photovoltaic potential at urban scale using BIM and LiDAR. *International Conference on Sustainable Infrastructure* 2017;2017:123–34.
- Suomalainen K, Wang V, Sharp B. Rooftop solar potential based on LiDAR data: bottom-up assessment at neighbourhood level. *Renew Energy* 2017;111:463–75. <https://doi.org/10.1016/j.renene.2017.04.025>.
- Martín-Jiménez J, Del Pozo S, Sánchez-Aparicio M, Lagüela S. Multi-scale roof characterization from LiDAR data and aerial orthoimagery: automatic computation of building photovoltaic capacity. *Autom Constr* 2020;109:102965. <https://doi.org/10.1016/j.autcon.2019.102965>.
- Thebault M, Desthieux G, Castello R, Berrah L. Large-scale evaluation of the suitability of buildings for photovoltaic integration: case study in greater Geneva. *Appl Energy* 2022;316:119127. <https://doi.org/10.1016/j.apenergy.2022.119127>.
- Dhamankar N, Kulkarni P, Dixit N. Estimating potential solar energy on rooftops using unmanned aerial vehicle. In: 2019 international conference on

- computational intelligence and knowledge economy (ICCIKE). IEEE; 2019. p. 275–8.
- [43] Polo J, García RJ. Solar potential uncertainty in building rooftops as a function of digital surface model accuracy. *Remote Sens* 2023;15:567. <https://doi.org/10.3390/rs15030567>.
- [44] Chen Y, Hong T, Piette MA. Automatic generation and simulation of urban building energy models based on city datasets for city-scale building retrofit analysis. *Appl Energy* 2017;205:323–35. <https://doi.org/10.1016/j.apenergy.2017.07.128>.
- [45] Zhang L, Zhang L. Deep learning-based classification and reconstruction of residential scenes from large-scale point clouds. *IEEE Trans Geosci Remote Sens* 2017;56:1887–97.
- [46] Yao Y, Luo Z, Li S, Fang T, Quan L. MVSNet: Depth Inference for Unstructured Multi-view Stereo. 2018. <https://doi.org/10.48550/ARXIV.1804.02505>.
- [47] Yao Y, Luo Z, Li S, Shen T, Fang T, Quan L. Recurrent MVSNet for High-resolution Multi-view Stereo Depth Inference. 2019. <https://doi.org/10.48550/ARXIV.1902.10556>.
- [48] Gu X, Fan Z, Dai Z, Zhu S, Tan F, Tan P. Cascade Cost Volume for High-Resolution Multi-View Stereo and Stereo Matching. 2019. <https://doi.org/10.48550/ARXIV.1912.06378>.
- [49] Yang G, Zhou X, Gao C, Chen X, Chen BM. Learnable cost metric-based multi-view stereo for point cloud reconstruction. *IEEE Trans Ind Electron* 2024;1–10. <https://doi.org/10.1109/TIE.2023.3337697>.
- [50] Zhang C, Li Z, Jiang H, Luo Y, Xu S. Deep learning method for evaluating photovoltaic potential of urban land-use: a case study of Wuhan. *China Applied Energy* 2021;283:116329. <https://doi.org/10.1016/j.apenergy.2020.116329>.
- [51] Mathews I, Sofia S, Ma E, Jean J, Laine HS, Siah SC, et al. Economically sustainable growth of perovskite photovoltaics manufacturing. *Joule* 2020;4:822–39. <https://doi.org/10.1016/j.joule.2020.01.006>.
- [52] Liu J, Wang M, Peng J, Chen X, Cao S, Yang H. Techno-economic design optimization of hybrid renewable energy applications for high-rise residential buildings. *Energy Convers Manag* 2020;213:112868. <https://doi.org/10.1016/j.enconman.2020.112868>.
- [53] Zhou Q-Y, Neumann U. 2.5 d dual contouring: A robust approach to creating building models from aerial lidar point clouds. *Computer Vision–ECCV 2010: 11th European conference on computer vision, Heraklion, Crete, Greece, September 5–11, 2010, proceedings, part III 11*. Springer; 2010. p. 115–28.
- [54] Li M, Wonka P, Nan L. Manhattan-world urban reconstruction from point clouds. *Computer Vision–ECCV 2016: 14th European conference, Amsterdam, the Netherlands, October 11–14, 2016, proceedings, part IV 14*, Springer; 2016, p. 54–69.
- [55] Li Q, Monticelli C, Zanelli A. Life cycle assessment of organic solar cells and perovskite solar cells with graphene transparent electrodes. *Renew Energy* 2022; 195:906–17. <https://doi.org/10.1016/j.renene.2022.06.075>.
- [56] Li T, Li Q. Virtual reality in historic Urban District renovation for enhancing social and environmental sustainability: a case of Tangzixiang in Anhui. *Sustainability* 2024;16:2665. <https://doi.org/10.3390/su16072665>.